Are fjords sources or sinks of CO_2? A study of air-sea CO_2 fluxes in Nootka Sound, B.C.

Claire Knox[1]

[1] University of Washington, School of Oceanography, Box 357940, Seattle, Washington, 98195-7940

cesk@uw.edu

31 May 2015

Acknowledgements

I am enormously grateful to Dr. Julian Sachs for being an encouraging, knowledgeable, and enthusiastic mentor. Thank you to Dr. Arthur Nowell for providing spiritual guidance throughout this process who always reminded me to breathe and not panic. Thank you to all of the faculty, students, and crew who assisted during fieldwork, specifically Kathy Newell, Dave Thoreson, Una Miller, Matthew Morris, and Danielle Dhanens. Thank you to the numerous people who provided their help and support including Dr. Miles Logsdon, Jaclyn Saunders, Gwenn Miller Hennon, Megan Schatz, Caroline Belleman, and Lauren Brandkamp. Finally, thank you to the University of Washington School of Oceanography who provided financial and logistical support allowing the entire class of 2015 to explore their passion through individual senior thesis projects.

Abstract

Carbon dioxide, an important atmospheric greenhouse gas, has increased approximately 40% in the past 200 years due to anthropogenic activity. As a result of this, the global carbon cycle has been thrown out of its pre-industrial period state as the ocean has begun to take up more anthropogenic carbon dioxide (CO_2) across the air-sea interface. In order to predict the future climate, carbon cycle, and marine biogeochemistry, one needs to quantify the movement of atmospheric CO_2 into the ocean. This study examined the CO_2 fluxes in an unstudied coastal region in Nootka Sound, British Columbia, Canada. The mean ΔpCO_2 was -126.9 μatm and mean influx of 3.2 mmol C m^{-2} d^{-1}. Assuming this is representative of the entire year, the annual carbon uptake would be 1.2 mol C m^{-2} yr^{-1} or 14.0 g C m^{-2} yr^{-1} which is equivalent to uptake in the North Pacific Ocean at ~50^0 latitude. While fjords only cover 0.1% of the ocean's surface area, this study suggests that they are an important component of the global carbon cycle.

Introduction

Since the industrial revolution, atmospheric CO_2 concentrations have increased from 280 ppm to 396 ppm due to deforestation and fossil fuel burning (Sabine et al. 2004). This rise is a concern as CO_2 is an effective greenhouse gas, absorbing and re-emitting back to the earth's surface radiation that would have originally escaped the atmosphere. Approximately half of anthropogenic CO_2 remains in the atmosphere with the other half being taken up in near equal proportions by the terrestrial biosphere and the ocean (Sabine et al. 2004). In 2000, the ocean drew down 2±1 Pg C yr^{-1} which includes the pre-industrial steady-state and recent anthropogenic flux. The uptake occurred in the subtropical and middle latitudes while the polar and equatorial latitudes released carbon dioxide (Fig. 1) (Takahashi et al. 2009). While the spatial distribution of carbon dioxide fluxes across the air-sea boundary is well defined for the open ocean, coastal systems are severely understudied due to high spatial and temporal heterogeneity (Torres et al. 2011).

Coastal systems have a disproportionally high ratio of carbon and nutrients to surface area due to large terrestrial inputs of organic matter and nutrients (Borges 2005). They make up 10-15% of the ocean surface area yet sequester 40% of the oceanic carbon, functioning as the main export of organic matter to the deep sea which regulates the CO_2 uptake (Emerson and Hedges 2008; Muller-Karger et al. 2005). In 2005, Borges sought to quantify the contributions of eight different coastal systems by integrating 44 studies and up-scaling the results to determine the air-sea CO_2 fluxes over the coastal ocean (26 x 10^6 km^2). If estuaries and salt marshes were not considered in the up-scaling calculation, the coastal ocean behaves as a sink for atmospheric CO2 resulting in an uptake of 1.17 mol C m^{-2} yr^{-1} and increasing the global ocean uptake by 24%. If estuaries and salt marshes are considered, the coastal ocean behaves as a source for

atmospheric CO2 resulting in an efflux of 0.38 mol C m^{-2} yr^{-1} decreasing the global ocean uptake by 12% (Borges 2005). While the lack of adequate data coverage is notable, the study indicates the importance of highly active coastal oceans on biogeochemical cycling.

Nootka Sound is located along the west side of Vancouver Island, British Columbia, Canada at ~50^0 N. In winter, Nootka Sound is characterized by decreased daylight hours, strong weather systems, and lower salinity due to large river water fluxes from precipitation (Dodimead 1984). The primary objective of this study is to determine if Nootka Sound's inlets are a source or sink for atmospheric CO_2. To determine if it is a source or sink, atmospheric CO_2 was measured and oceanic CO_2 was calculated from multiple measured parameters. Once these are known, the flux can be calculated using the wind speed, Schmidt number which is the ratio of kinematic viscosity of seawater to its molecular diffusivity, and the gas solubility which is dependent on temperature and salinity (Emerson and Hedges 2008). In Nootka Sound, an uptake of CO_2 is predicted due to the high wind speed, low temperature, and low salinity. Also, a spatial distribution of decreasing uptake with distance from the freshwater input is anticipated because the freshwater will be colder, less saline, and potentially adding nutrients near the river mouth.

In addition to the primary objective, a secondary objective is to determine if the biological community is contributing to the CO_2 flux. In order to address this question, oxygen concentrations must be measured to determine if the surface layer is net heterotrophic or photosynthetic. Due to the expected uptake of CO_2, the water should be super-saturated with oxygen due to photosynthesis by primary producers aiding in the drawdown of CO_2.

For comparison, Torres et al. (2011) studied air-sea CO_2 fluxes along the coast of Chile. They determined that there was an efflux of CO_2 along the coast due to upwelling and an influx of CO_2 in the fjords. During austral winter in Penguin and Europa Fjords (~50^0S), there was an

uptake of CO_2 with the colder and less saline inner fjord waters having a lower partial pressure of CO_2 (pCO_2) than the warmer and saltier water at the fjord's entrance. There was also a positive correlation of surface pCO_2 with temperature and salinity.

In the future, it is predicted that the ocean CO_2 sink will increase while the biosphere will become a source. The uncertainty in this statement arises from not knowing all of the current sources and sinks especially in the coastal systems (Gruber et al. 2009). In order to predict future climate change, marine biogeochemistry, and global carbon cycle, we must understand the movement of atmospheric CO_2 into the ocean, especially in the highly variable coastal zone.

Methods

Study Site

Nootka Sound is located on the west coast of Vancouver Island, British Columbia, Canada. It is comprised of three major inlets: Muchalat, Tlupana, and Tahsis. This study focuses on Muchalat and Tahsis Inlets. Muchalat Inlet is 55 km long with an average depth of 220 m. Near the mouth of the inlet is a sill restricting the depth to 55 m. In December, the Gold River located away from the inlet entrance reaches maximum discharge of freshwater. Tahsis Inlet is 38 km long with an average depth of 135 m and sill depth of 50 m (Dodimead 1984). Tahsis Inlet is connected to Esperanza Inlet to the west via Hecate Channel (Fig. 2).

Overview

During 13-17 December 2014, sampling occurred in Nootka Sound, Canada using the R/V Weelander, a small boat deployed from the deck of the R/V Thomas G. Thompson. Each day the R/V Weelander was deployed at 0800 and returned by 1600 to sample during daylight hours. 74 samples were taken every 0.65-0.8 nautical miles across Muchalat, Tlupana, and Tahsis Inlets. Due to time and funding constraints, DIC and alkalinity samples were only

measured at 18 stations in Muchalat Inlet and 12 stations in Tahsis Inlet. These stations were chosen to canvas the entire spatial range as well as represent the range in salinity and temperature.

Field Sampling and Shipboard Analysis

Upon arrival at the sampling site, the coordinates were recorded from the R/V Weelander's Garmin GPS System. Next the YSI Data Sonde 556 was deployed to measure temperature and salinity from the side of the vessel approximately 10 cm below the surface. It was held until the readings stabilized approximately 3 minutes after deployment and values were recorded. While the YSI Data Sonde was equilibrating, water was collected for dissolved oxygen, alkalinity, and dissolved inorganic carbon (DIC) analysis. For dissolved oxygen, 125 ml bottles with a ground glass stopper were placed a few centimeters below the surface to allow the water to slowly fill the bottle entirely (Shamberger et al. 2011). They were then fixed with 1 ml of $MnCl_2$ and 1 ml of NaOH-NaI and stoppered for later analysis on the R/V Thompson. They were analyzed 12-36 hours post-collection following the Winkler titration method using a Dosimat 665 (Carpenter 1965). Water for DIC and alkalinity analysis were collected similarly to the dissolved oxygen however in two 250 ml or one 500 ml bottles with a ground glass stopper. They were filled until 1 cm headspace existed below the neck equating to roughly 1% of the total bottle volume. 100 µl of mercuric chloride per 250 ml seawater was added to eradicate any biological activity. Finally, the stoppers were covered in a thin line of Apiezon M grease, stoppered using a twisting motion to distribute the grease, and encased in a rubber band (Shamberger et al. 2011; NOAA:PMEL 2010). Upon arrival at the R/V Thompson each day, the samples were transferred to a refrigerator to inhibit thermal expansion.

Post-Cruise Lab and Analysis

On return to the University of Washington, DIC and alkalinity samples were analyzed. Alkalinity samples were measured by Dongsen Xue, manager of the UW Analytical Service Center in the School of Forestry, following the EPA 310.1 method (US EPA 1978). DIC samples were analyzed in the UW Center for Environmental Genomics using an Apollo Scitech DIC analyzer model AS-C3 with LI-7000 attached.

Calculations

The fluxes of CO_2 across the air-sea interface can be calculated using the gas transfer velocity of CO_2, the solubility of CO_2 in seawater, and the difference between oceanic pCO_2 and atmospheric pCO_2. The oceanic pCO_2 was calculated using CO_2Sys (Pierrot et al. 2006).

$$F = k * S * \Delta pCO_{2\,(sw\text{-}atm)}$$

$$\Delta pCO_{2\,(sw\text{-}atm)} = pCO_{2\,sw} - pCO_{2\,atm}$$

$$k = (0.222*U^2 + 0.333*U)(Sc/600)^{-0.5}$$

The pCO_2 is the partial pressure of CO_2 in the seawater or atmosphere. Values for atmospheric CO_2 were obtained from Environment Canada's Estevan Point station located on the southern entrance to Nootka Sound. Atmospheric CO_2 was measured aboard the R/V Weelander using a pSense-Plus handheld non-dispersive infrared sensor however the data was later deemed biased due to the exhaust of the outboard engine and anthropogenic influence. The $\Delta pCO_{2\,(sw\text{-}atm)}$ is the difference between the calculated oceanic pCO2 and measured atmospheric pCO_2. The sign of this value determines the direction of gas diffusion with a positive ΔpCO_2 representing an outgassing of CO_2. The S term or solubility of CO_2 in seawater is dependent on the temperature and salinity of the seawater (Takahashi et al. 2009). The *k* term is the gas transfer velocity of CO_2 and is dependent on the wind speed U and the Schmidt number Sc (Nightingale et al. 2000).

Percent dissolved oxygen saturation was calculated as a function of temperature and salinity using equations defined by Weiss (1970).

Results

Salinity and Temperature

The surface water in Muchalat Inlet was fresher than Tahsis Inlet due to the Gold River discharge. The salinity ranged from 0.52-8.70 with an average of 4.17. Tahsis Inlet had a greater salinity range of 7.80-21.5 with an average of 14.49 (Fig. 2). Muchalat Inlet was colder than Tahsis Inlet with an average temperature of 6.69 ^{o}C relative to 7.97 ^{o}C (Fig. 3). For both inlets, temperature and salinity decreased with distance away from the inlet entrance.

Dissolved Inorganic Carbon

Muchalat Inlet had less DIC with a minimum of 239 μmol kg^{-1}, maximum of 615 μmol kg^{-1}, and mean of 382 μmol kg^{-1}. Tahsis Inlet had greater DIC with a minimum of 467 μmol kg^{-1}, maximum of 1406 μmol kg^{-1}, and mean of 947 μmol kg^{-1}.

Alkalinity

Muchalat Inlet had lower alkalinity with a minimum of 206 μeq kg^{-1}, maximum of 623 μeq kg^{-1}, and mean of 395 μeq kg^{-1}. Tahsis Inlet had greater alkalinity with a minimum of 507 μeq kg^{-1}, maximum of 1144 μeq kg^{-1}, and mean of 993 μeq kg^{-1}.

Dissolved Oxygen

All measured surface water was undersaturated in dissolved oxygen. Muchalat Inlet had a higher mean saturation of 62.2% while Tahsis Inlet had a mean saturation of 57.6%. The overall mean saturation of all three inlets was 60.0% (Fig. 4).

ΔpCO_2

Tahsis Inlet was an overall sink for atmospheric CO_2 while Muchalat Inlet was a source and a sink with the lower salinity waters typically being a source of CO_2 to the atmosphere (Fig. 5). Tahsis Inlet had a mean ΔpCO_2 of -169.3 μatm while Muchalat Inlet had a mean ΔpCO_2 of -84.5 μatm (Fig. 6).

Wind

Wind speed was measured using the R/V Thompson MET data system. Daily instantaneous wind speed ranged from 0-16.77 m s^{-1} while daily mean wind speed ranged from 2.02-5.73 m s^{-1} (Table 1).

Flux

The mean flux of CO_2 in Muchalat Inlet was -4.7 mmol C m^{-2} d^{-1} and -1.7 mmol C m^{-2} d^{-1} in Tahsis Inlet.

Discussion

The circulation of estuarine systems that are deep and strongly stratified can be simplified as a two-layer model (Stigebrandt 1981). The upper layer is caused by freshwater runoff from rivers and moves away from the river source. The deep layer has oceanic origins and can be subdivided into two more layers, the intermediate water and deep water. The intermediate water is flowing in the opposite direction of the river runoff while the deep water is stagnant and trapped by the sill (Fig. 7). In winter, Muchalat Inlet strongly resembles the two-layer model due to Gold River's large freshwater runoff and strong gradient of salinity with depth. The Gold River discharges the greatest quantities in winter (mid-October to mid-January) with the maximum discharge occurring in mid-December during the sampling period (Fig. 8) (Government of Canada 2015). As the freshwater moves away from the river source, it slowly mixes with more saline water due to wind-induced vertical mixing. This produced the

comparatively freshwater in Muchalat Inlet with a measured salinity of 0.50-1.0 near the Gold River mouth compared to Tahsis Inlet's minimum surface salinity of 7.80. Tahsis Inlet does not have a large, main river source and instead has a multitude of small rivers creating a more complex and unknown circulation pattern.

In Muchalat and Tahsis Inlets, the alkalinity increased away from the freshwater sources suggesting the freshwater had low alkalinity and the seawater had high alkalinity. There was no spatial pattern of DIC in Muchalat Inlet; however in Tahsis Inlet DIC increased two fold moving south, towards the entrance of the inlet. While this may be a function of the increasing proportion of seawater, it could also be a function of Tahsis Inlet's circulation. Tahsis Inlet connects to a network of other inlets to the west via the Hecate Channel. This introduces the potential for surface water from other inlets to enter Tahsis Inlet via Hecate Channel. The larger drainage area of these combined inlets could be supplying more quantities of minerals, soil, and terrestrial carbon that could contribute to the 2.5 times greater concentration of DIC and alkalinity in Tahsis Inlet. As DIC and alkalinity are the dominant variables in calculating ΔpCO_2, it is important to evaluate the sources and circulation in both inlets.

ΔpCO_2 can be considered an indicator for air-sea CO_2 exchange as it signifies a gradient or the potential for CO_2 to move across the boundary. While Tahsis Inlet had a two fold greater ΔpCO_2, the mean flux was only one-third of Muchalat Inlet's mean CO_2 flux. This can be attributed to the wind speed which was almost three times greater in Muchalat Inlet than Tahsis Inlet during sampling. This resulted in a CO_2 flux of -4.7 mmol C m^{-2} d^{-1} in Muchalat Inlet and -1.7 mmol C m^{-2} d^{-1} in Tahsis Inlet. This illustrates the importance of wind speed for gas exchange across the air-sea boundary.

Assuming winter conditions persists for three months and the average of these two fluxes is a good representation of annual winter CO_2 fluxes, Nootka Sound is absorbing 294.4 mmol C m^{-2} every winter. If these winter fluxes are representative of the entire year, the flux can be scaled to an annual Nootka Sound carbon uptake of 1.2 mol C m^{-2} yr^{-1} or 14.0 g C m^{-2} yr^{-1}. This value is comparable to the North Pacific Ocean's uptake at ~50^0 as well as another study on global coastal air-sea CO_2 fluxes (Fig. 1, Fig. 9) (Takahashi et al. 2009; Dai et al. 2013). It is important to note that these conditions are extremely unlikely to persist throughout the entire year. In the summer freshwater runoff significantly decreases, surface water would be warmer decreasing gas solubility, the water column would be more thermally stratified, wind speed would decrease, and primary productivity would not be limited by solar radiation.

The secondary objective of this study was to determine if the biological community is contributing to the CO_2 flux. It was hypothesized that the water would be supersaturated in oxygen while being a sink for atmospheric CO_2 due to primary production. The water in all three inlets was undersaturated while the water was a sink for atmospheric CO_2. While this counteracts my secondary hypothesis, I can conclude that primary production is not a factor in driving CO_2 fluxes in winter. The likely reason is that low rates of primary production characterized the ecosystem due to insufficient solar radiation as this study was conducted two weeks prior to winter solstice, the shortest day of the year. Gonzalez et al. (2010) found that the seasonal variability in freshwater discharge and solar radiation directly affected the pelagic communities in Reloncaví Fjord, a Patagonian fjord. The vertical flux of particulate organic carbon increased two fold while the primary production increased two orders of magnitude between winter to spring due to the higher solar radiation and extended photoperiod.

Sources of error

There are many potential sources of error with this experiment that could have influenced the calculated CO_2 fluxes. The two greatest sources are wind speed and assuming that all water measurements were taken at the same depth (Table 2). First, wind speed was measured onboard the R/V Thompson which was moving independently of the R/V Weelander from which all other measurements were made. Most of the time the two vessels were kept within a few kilometers but at times were up to 20 km apart. This introduces a large quantity of uncertainty in the calculated fluxes as wind speed was the most important variable, outweighing the ΔpCO_2 and solubility of CO_2 in seawater variables. Secondly, the probe measuring water parameters and the water collection for DIC and alkalinity analysis was happening simultaneously however may not have been capturing the identical water mass. The probe was lowered until fully submerged which was ~10 cm below the surface. The bottles were tilted into the water roughly ~5 cm below the surface allowing water to slowly diffuse in. This could result in water samples anywhere in the upper 10 cm. Depending on how distinct the surface water was from the water below, this method could have been sampling two different water masses.

In addition to the two main sources of error, analytical techniques could have influenced the CO_2 flux calculations. The alkalinity analysis had a precision of ±20 μeq kg^{-1} and DIC analysis had a precision of ±10 μmol kg^{-1}. Another potential source of error is the 1% headspace left in each DIC and alkalinity sample bottle. This small volume of air could have increased the DIC concentration due to CO_2 diffusing into the water between the collection and analysis period. This would have no effect on the alkalinity but would increase the DIC thus increase the ΔpCO_2. If this did occur it would increase the CO_2 flux calculation by a small quantity. With only a 1% headspace, this is proportionally insignificant compared to other sources of uncertainty like the wind speed measurements.

Future Research

While fjords only cover 0.1% of the ocean's surface area, they play an important role in biogeochemical cycling. More research to understand their role in carbon cycling at the surface and at depth is vital. Future air-sea CO_2 studies could utilize emerging technology such as autonomous oceanographic floats. A recent paper by Smith et al. (2015) suggests that fjords are responsible for 11% of marine organic carbon burial resulting in 18 Mt C buried per year yet more research is necessary to confirm the role of fjords in carbon cycling.

References

Borges, A.V. 2005. Do we have enough pieces of the jigsaw to integrate CO_2 fluxes in the coastal ocean? Estuaries. **28**(1): 3-27.

Carpenter, J. H. 1965. The Chesapeake Bay Institute Technique for the Winkler dissolved oxygen method. Limnol. Oceanogr. **10**: 141–143.

Dai, M., Z. Cao, X. Guo, W. Zhai, Z. Liu, Z. Yin, Y. Xu, J. Gan, J. Hu, C. Du. 2013. Why are some marginal seas sources of atmospheric CO_2. Geophys. Res. Lett. **40**: 2154-2158.

Dodimead, A.J.1984. A review of some aspects of the physical oceanography of the continental shelf and slope waters off the west coast of Vancouver Island, British Columbia. Canadian Manuscript Report of Fisheries and Aquatic Sciences No. 1773.

Emerson, S. and J. Hedges. 2008. Chemical oceanography and the marine carbon cycle. Cambridge University Press.

Gonzalex, H.E. M.J. Calderon, L. Castro, A. Clement, L.A. Cuevas, G. Daneri, J.L. Iriarte, L. Lizarraga, R. Martinez, N. Silva, C, Carrasco, C. Valenzuela, C.A. Vargas, C. Molinet. 2010. Primary production and plankton dynamics in the Reloncavi Fjord and interior Sea of Chiloe, Northern Patagonia, Chile. Mar. Ecol. Prog. Ser. **402**: 13-30.

Government of Canada. 2015. Real-time hydrometric data graph for Gold River below Ucona River. https://wateroffice.ec.gc.ca/report/report_e.html?type=realTime&stn=08HC001

Gruber, N., M. Gloor, S.E. Mikaloff Fletcher, S.C. Doney, S. Dutkiewicz, M.J. Follows, M. Gerber, A.R. Jacobson, F. Joos, K. Lindsay, D. Menemenlis, A. Mouchet, S.A. Muller, J.L. Sarmiento, T. Takahashi. 2009. Oceanic sources, sinks, and transport of atmospheric CO_2. Global Biogeochem. Cy. **23**(GB1005).

Muller-Karger, F.E., R. Varela, R. Thunell, R. Luerssen, C. Hu, J.J. Walsh. 2005. The importance of continental margins in the global carbon cycle. Geophys. Res. Lett. **32**(L01602).

National Oceanic and Atmospheric Association (NOAA): Pacific Marine Environmental Laboratory (PMEL). 2010. Inorganic carbon sampling. http://www.pmel.noaa.gov/co2/files/dic_sample_technique_revised_5-17-10.pdf

Nightingale, P.D., G. Malin, C.S. Law, A.J. Watson, P.S. Liss, M.I. Liddicoat, J. Boutin, R.C. Upstill-Goddard. 2000. In situ evaluation of air-sea gas exchange parameterizations using novel conservative and volatile tracers. Global Biogeochem. Cy. **14**(1): 373-387.

Sabine, C.L., R.A. Feely, N. Gruber, R.M. Key, K. Lee, J.L. Bullister, R. Wanninkhof, C.S. Wong, D.W.R. Wallace, B. Tilbrook, F.J. Millero, T. Peng, A. Kozyr, T. Ono, A.F. Rios. 2004. The oceanic sink for anthropogenic CO_2. Science. **305**(5682): 367-371.

Shamberger, K.E.F., R.A. Feely, C.L. Sabine, M.J. Atkinson, E.H. DeCarlo, F.T. Mackenzie, P.S. Drupp, D.A. Butterfield. 2011. Calcification and organic production on a Hawaiian coral reef. Mar. Chem. **127**: 64-75.

Smith, R.W., T.S. Bianchi, M. Allison, C. Savage, V. Galy. 2015. High rates of organic carbon burial in fjord sediments globally. Nat. Geosci. Advance online publication.

Stevenson, J.S. 1950. Geology and mineral deposits of the Zeballos mining camp. British Columbia Department of Mines.

Stigebrandt, A. 1981. A mechanism governing the estuarine circulation in deep, strongly stratified fjords. Cont. Shelf Res. **13**: 197-211.

Takahashi, T., S.C. Sutherland, R. Wanninkhof, C. Sweeny, R.A. Feely, D.W. Chipman, B. Hales, G. Friederich, F. Chavez, C. Sabine, A. Watson, D. Bakker, T. Schuster, N. Metzl,

H. Yoshikawa-Inoue, M. Ishii, T. Midorikawa, Y. Norjiri, A. Kortzinger, T. Steinhoff, M. Hoppema, J. Olafsson, T.S. Arnarson, B. Tilbrook, T. Johannessen, A. Olsen, R. Bellerby, C.S. Wong, B. Delille, N.R. Bates, H de Baar. 2009. Climatological mean and decadal change in surface pCO_2 and net sea-air CO_2 flux over the global ocean. Deep-Sea Res. **56**: 554-577.

Torres, R., S. Pantoja, N. Harada, H.E. Gonzalez, G. Daneri, M. Frangopulos, J.A. Rutlant, C.M. Duarte, S. Ruiz-Halpern, E. Majol, and M. Fukasawa. 2011. Air-sea CO_2 fluxes along the coast of Chile: From CO_2 outgassing in central northern upwelling waters to CO_2 uptake in southern Patagonian fjords. J. Geophys. Res. Oceans. **16**(C9): 1-17.

United States Environmental Protection Agency (US EPA); Office of Research and Development, Environmental Monitoring, and Support Laboratory. 1978. Alkalinity: Test Method 310.1.

Wanninkhof, R. 1992. Relationship between wind speed and gas exchange over the ocean. J. Geophys. Res. **97**(C5): 7373-7382.

Weiss, R.F. 1970. The solubility of nitrogen, oxygen, and argon in water and seawater. Deep-Sea Res. **17**: 721-735.

Table 1. The minimum, average, and mean wind speed (m s^{-1}) when sampling occurred. Muchalat Inlet sampling occurred on 13-14 December 2014 and Tahsis Inlet sampling occurred on 17 December 2014.

Date	Minimum Wind Speed (m s^{-1})	Maximum Wind Speed (m s^{-1})	Mean Wind Speed (m s^{-1})
13 Dec	0	14.51	5.73
14 Dec	0	16.77	5.45
17 Dec	0	9.723	2.02

Table 2. The sources of potential error affecting the calculated air-sea CO_2 fluxes.

Sources of Potential Error	Estimated Percentage Error
Temperature Measurement	<1%
Salinity Measurement	<1%
Alkalinity Measurement	<1%
DIC Measurement	2%
Wind Speed Measurement	25%
Schmidt Number of 660 Assumption	2%
Everything Measured at Same Depth Assumption	10%
Solubility Constant Assumption	<1%
CO2sys Calculator	2%

Figure 1

The global mean sea-air flux of carbon dioxide for 2000 in grams C m^{-2} yr^{-1} (Takahashi et al. 2009).

Figure 2

The spatial distribution of salinity across the three inlets of Nootka Sound: Tahsis Inlet (left), Tlupana Inlet (center), and Muchalat Inlet (right).

Figure 3

The surface temperature (^{o}C) plotted against the surface salinity in Muchalat Inlet (purple) and Tahsis Inlet (red).

Figure 4

The spatial distribution of percent saturation dissolved oxygen across the three inlets of Nootka Sound: Tahsis Inlet (left), Tlupana Inlet (center), and Muchalat Inlet (right). Percent dissolved oxygen saturation calculated as a function of temperature and salinity using equations defined by Weiss (1970).

Figure 5

The surface ΔpCO2 (μatm) plotted against the surface salinity. Muchalat Inlet (purple), Tahsis Inlet (red), and the open ocean sample taken at 1.2 m depth located 41 nautical miles away from the entrance to Nootka Sound (green).

Figure 6

The spatial distribution of ΔpCO_2 across Tahsis Inlet (left) and Muchalat Inlet (right). The sign of the ΔpCO_2 determines the direction of gas diffusion with a positive value representing an efflux and a negative representing an influx of atmospheric CO_2.

Figure 7

A sketch showing a vertical cross section along a fjord (Stigebrandt 1981).

Figure 8

Gold river discharge in $m^3\ s^{-1}$ from 1 January 2014 to 1 January 2015. The season of greatest discharge was from mid-October to mid-January with the maximum discharge occurring in mid-December (Government of Canada 2015).

Figure 9

Global annual CO_2 air-sea fluxes in coastal margins (Dai et al. 2013).

Fig. 1

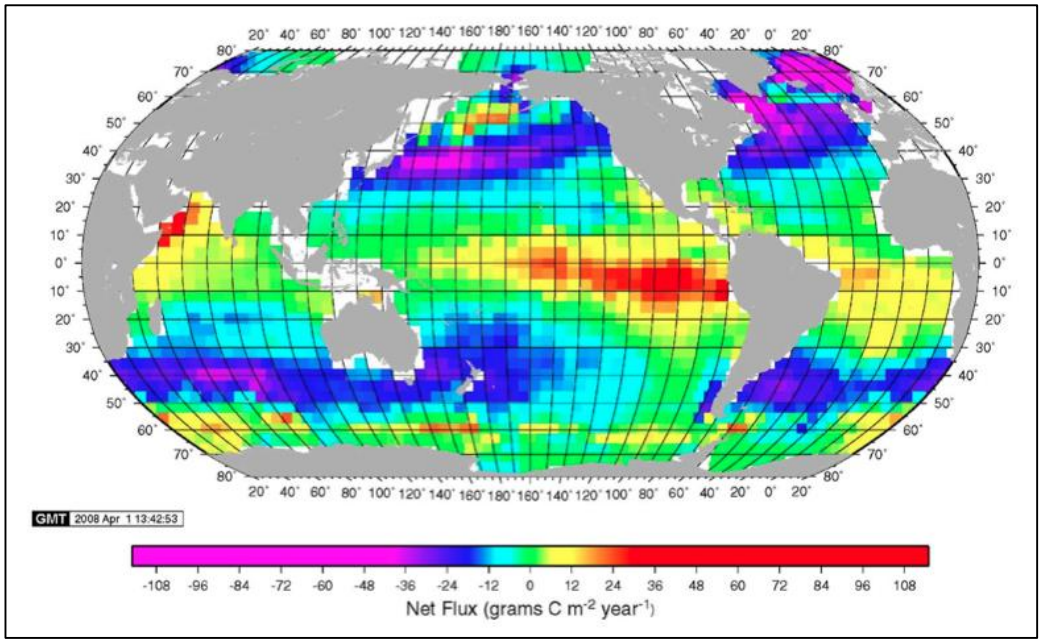
GMT 2008 Apr 1 13:42:53
-108 -96 -84 -72 -60 -48 -36 -24 -12 0 12 24 36 48 60 72 84 96 108
Net Flux (grams C m-2 year-1)

Fig. 2

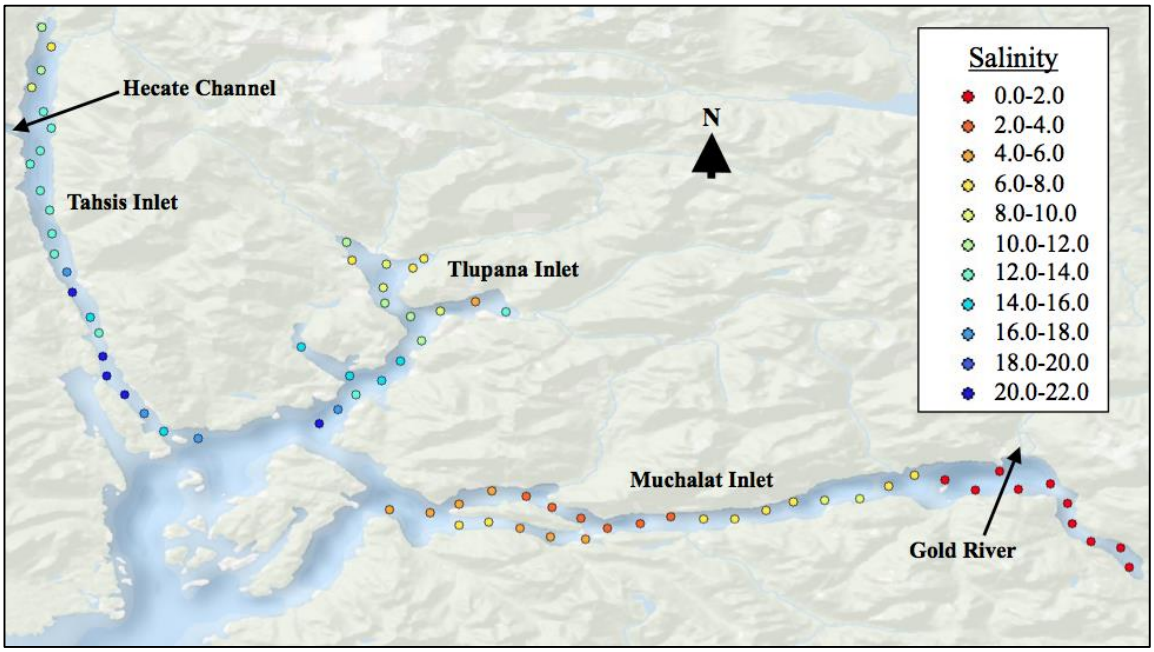
Hecate Channel
Tahsis Inlet
Tlupana Inlet
Muchalat Inlet
Gold River
N
Salinity
0.0-2.0
2.0-4.0
4.0-6.0
6.0-8.0
8.0-10.0
10.0-12.0
12.0-14.0
14.0-16.0
16.0-18.0
18.0-20.0
20.0-22.0

Fig. 3

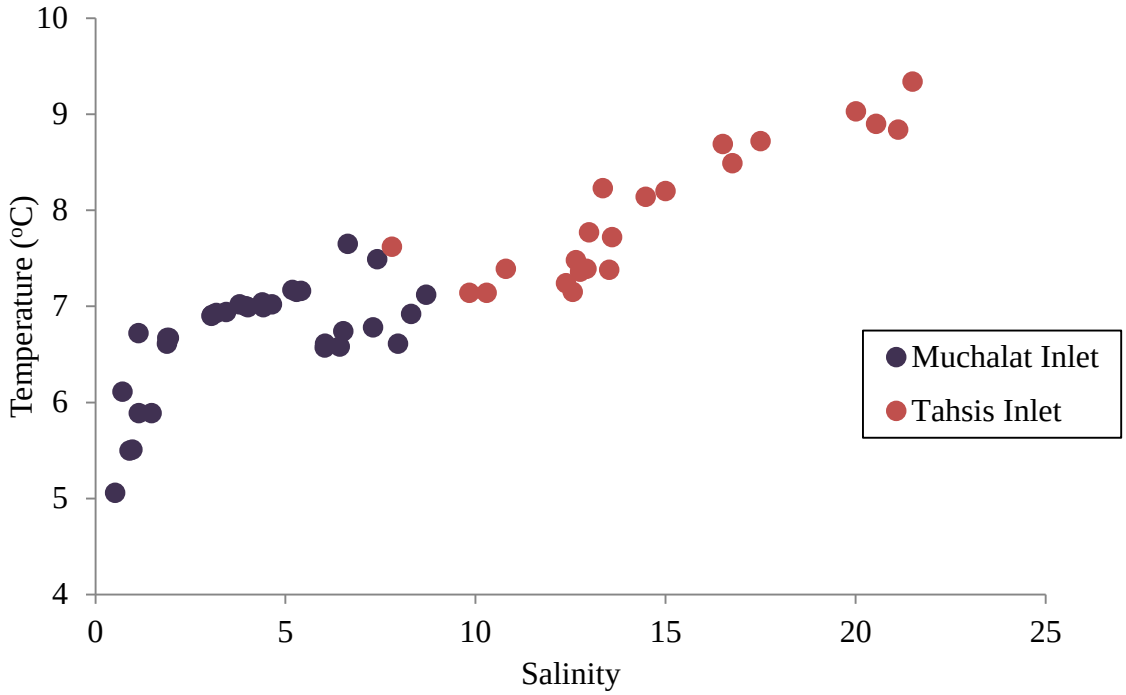
Temperature (°C)
10
9
8
7
6
5
4
0
5
10
15
20
25
Salinity
Muchalat Inlet
Tahsis Inlet

Fig. 4

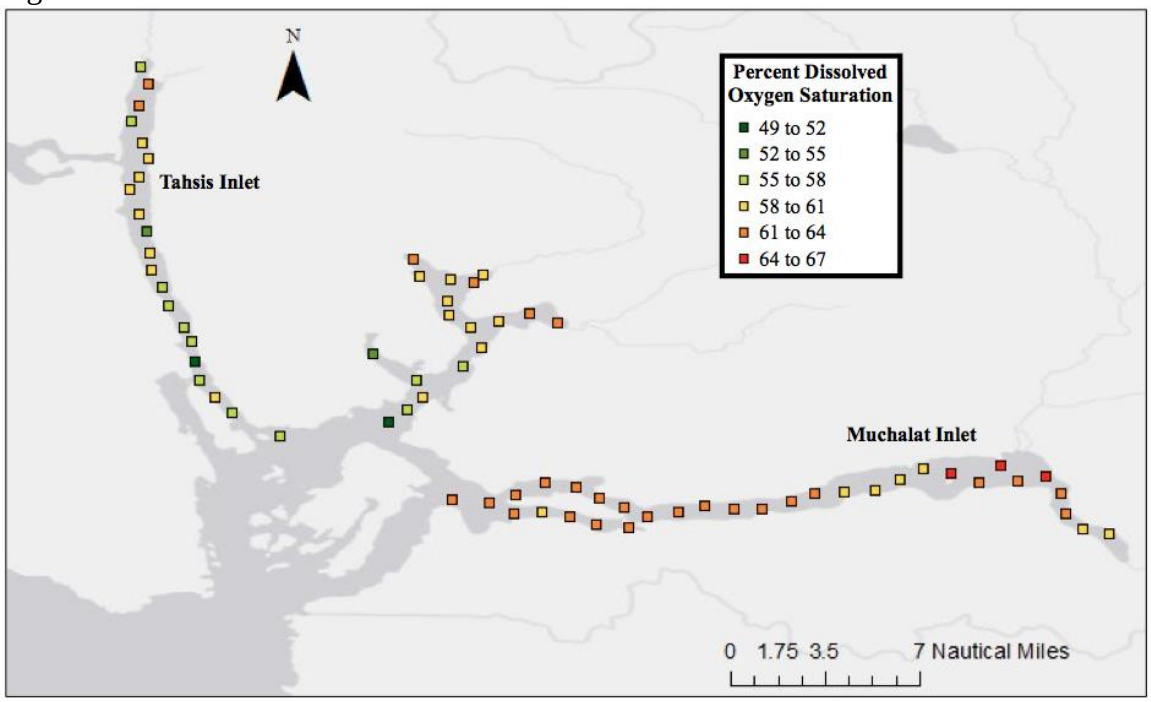
N
Percent Dissolved Oxygen Saturation
49 to 52
52 to 55
55 to 58
58 to 61
61 to 64
64 to 67
Tahsis Inlet
Muchalat Inlet
0 1.75 3.5 7 Nautical Miles

Fig. 5

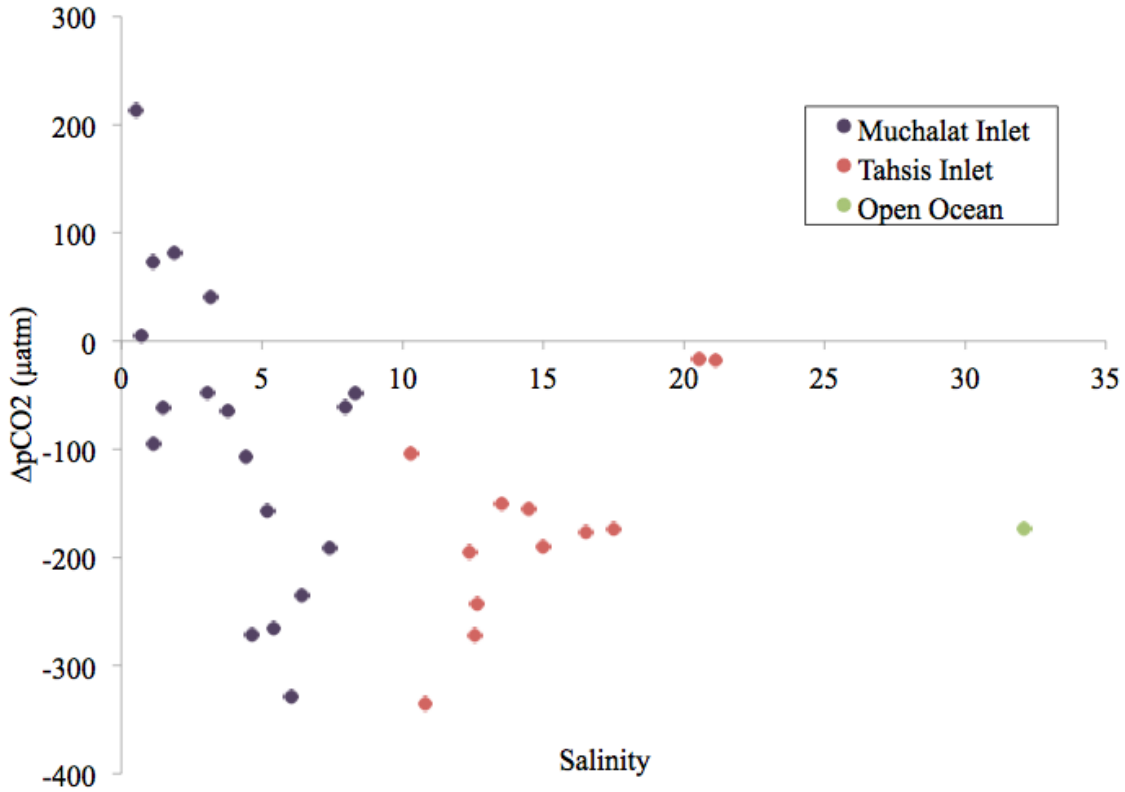
300
200
100
0
-100
-200
-300
-400
0
5
10
15
20
25
30
35
ΔpCO2 (µatm)
Salinity
Muchalat Inlet
Tahsis Inlet
Open Ocean

Fig. 6

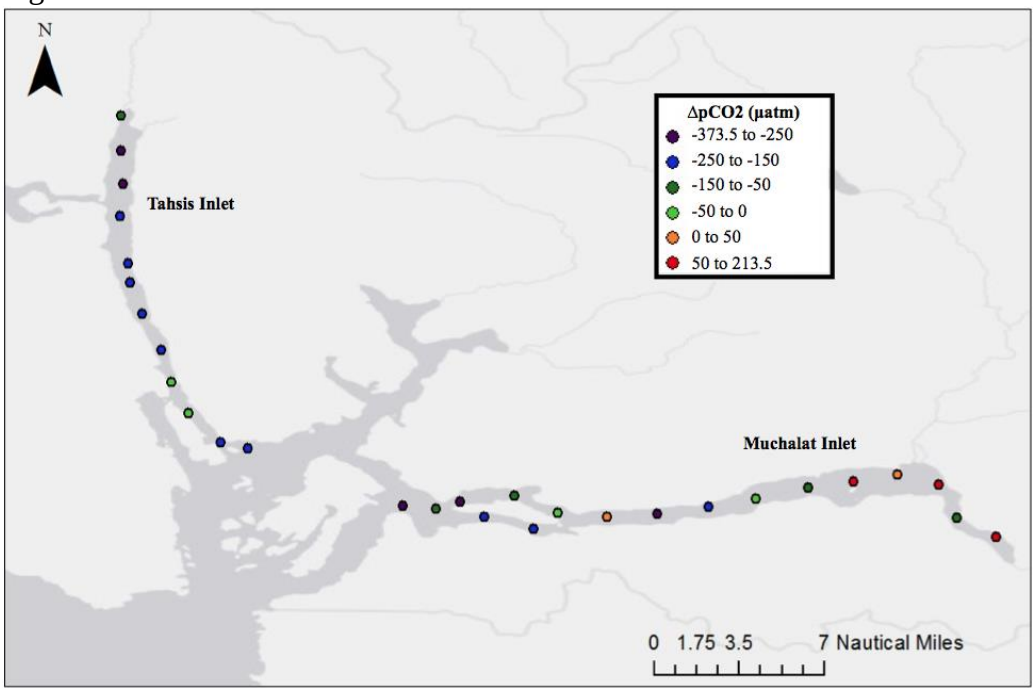
N
ΔpCO2 (µatm)
-373.5 to -250
-250 to -150
-150 to -50
-50 to 0
0 to 50
50 to 213.5
Tahsis Inlet
Muchalat Inlet
0 1.75 3.5 7 Nautical Miles

Fig. 7

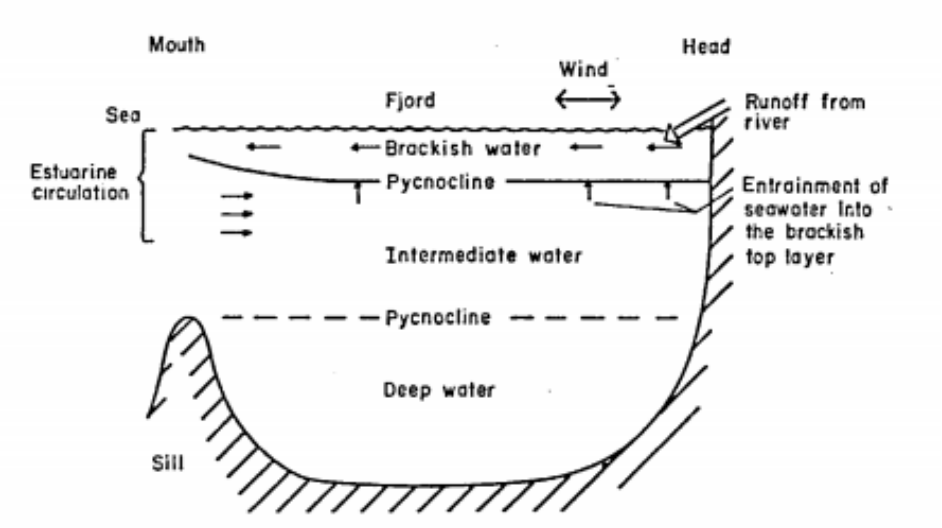
Mouth
Head
Wind
Fjord
Sea
Runoff from river
Brackish water
Estuarine circulation
Pycnocline
Entrainment of seawater into the brackish top layer
Intermediate water
Pycnocline
Deep water
Sill

Fig. 8

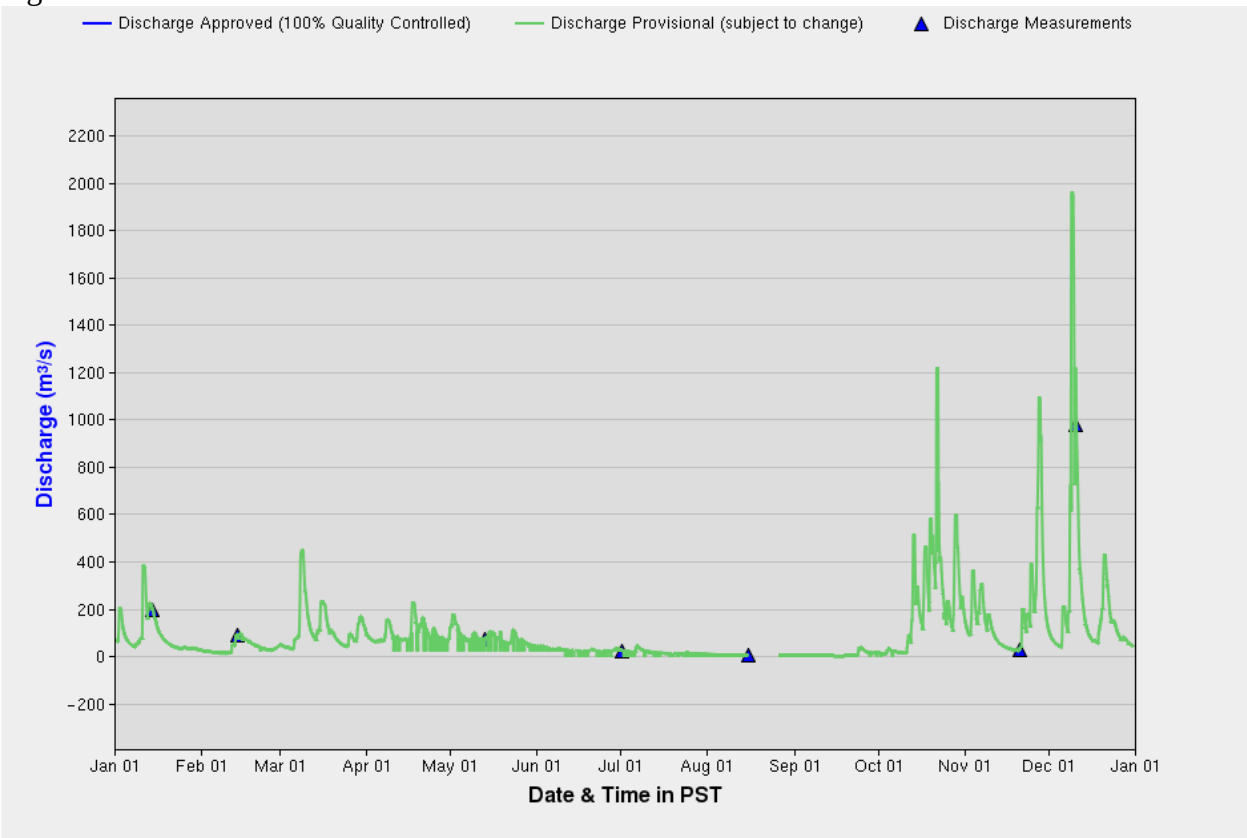
Discharge Approved (100% Quality Controlled)
Discharge Provisional (subject to change)
Discharge Measurements
Discharge (m³/s)
2200
2000
1800
1600
1400
1200
1000
800
600
400
200
0
-200
Jan 01
Feb 01
Mar 01
Apr 01
May 01
Jun 01
Jul 01
Aug 01
Sep 01
Oct 01
Nov 01
Dec 01
Jan 01
Date & Time in PST

Fig. 9

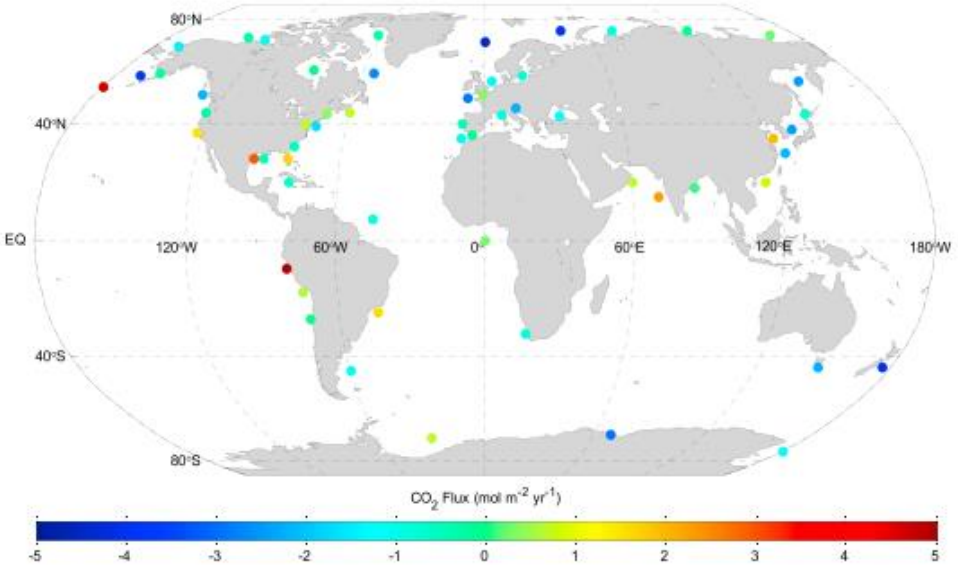
80°N
40°N
EQ
40°S
80°S
120°W
60°W
0°
60°E
120°E
180°W
CO2 Flux (mol m-2 yr-1)
-5
-4
-3
-2
-1
0
1
2
3
4
5